# Easy Estimation of Wheel Lift and Suspension Force for Novel High-Speed Robot on Rough Terrain

Jayoung Kim[1], Bongsu Jeon[2], Youngjin Kim[3] and Jihong Lee[4]

[1,2,3,4] Department of Mechatronics Engineering, Chungnam National University, Deajeon, South Korea
{[1]jaya, [4]jihong}@cnu.ac.kr

**Abstract.** In operation of high-speed wheeled robots on rough terrain, it is significantly important to predict or measure the interaction between wheel and ground in order to maintain optimal maneuverability. Therefore, this paper proposes an easy way to estimate wheel lift and suspension force of a high-speed wheeled robot on uneven surfaces. First of all, a high-speed robot which has six wheels with individual steer motors was developed and the body of the robot is connected to each wheel by semi-active suspensions. In a sensor system, potentiometers which can measure angle of arms are mounted at the end of arms and it has a critical role to estimate wheel lift and suspension force. A simple dynamic equation of spring-damper system is used to estimate the suspension force and the equation is calculated in terms of the suspension displacement by measured angle of arms because the suspension displacement is a function of arm angle in boundary of kinematic model of body-wheel connection. Also, wheel lift can be estimated using the arm angle. When the robot keeps initial state without normal force, the arm angle is set as zero point. When the wheels get the normal force, the link angle is changed to higher value than zero point. And also, if a wheel does not contact to a ground, then the suspension force goes toward the negative direction as a value. Therefore, if wheel lift happens while driving, the arm angle will follow the zero point or the suspension force will indicate a negative value. The proposed method was validated in ADAM simulations. And the results of the performance were verified through outdoor experiments in an environment with an obstacle using a developed high-speed robot.

## 1 Introduction

Research on outdoor robotic vehicles has received significant attention for important tasks for exploration, reconnaissance, rescue, etc. In actual applications on outdoor environments, especially rough terrains, it is hard to automatically operate outdoor vehicles or robots because there are lots of elements to put them in dangerous situations such as overturn or wheel stuck. Accordingly, it is a big issue to optimize wheel traction [1, 2] and stability [3, 4] of vehicles on rough terrains and to estimate suspension force of vehicles for achieving the aims since suspension force is a variable used in order to control traction and to evaluate stability of vehicles [1-10]. Suspension force can be expressed as normal force acting on wheel and body. In previous studies, fully-dynamic models of vehicles or robots are applied to estimate the normal force [2-10]. However, it is not easy to derive the dynamic models and it is a laborious task to acquire accurate values of normal force in estimation system based on the dynamic models since the dynamic models include model uncertainty by complex terrain conditions, thereby robot states cannot be correctly estimated in real-time. And also, when it happens to take wheel off from ground (wheel lift) in case of high-speed driving on rough terrains, it is impossible to predict robot states and it can be confronted with a hazardous situation. Therefore, this paper proposes an easy way to estimate wheel lift and suspension force of a high-speed wheeled robot on uneven surfaces. In this paper, inexpensive potentiometer was only employed to measure angle of arms which is necessary to estimate wheel lift and suspension force in this simple method.

## 2 Estimation of Suspension Force and Wheel Lift

### 2.1 Caleb9; Omnidirectional High-speed Rough Terrain Robot

In this paper, an outdoor wheeled robot called Caleb9 was developed as shown in Fig. 1. Caleb9 has six in-wheel motors for driving and six BLDC motors for steering. Semi-active suspensions which can automatically adjust damping force are mounted for connection between wheel and body, independently. Arms of Caleb9 were designed as a structure of four-bar linkage in order to well overcome obstacles of a surface. Also, brake modules are attached to each wheel for rapidly stopping wheels. Caleb9 controls each driving motor to optimize wheel traction (Terrain-adaptive Slip Control [1]), steering motor to keep desired steering angle (Position Control), semi-

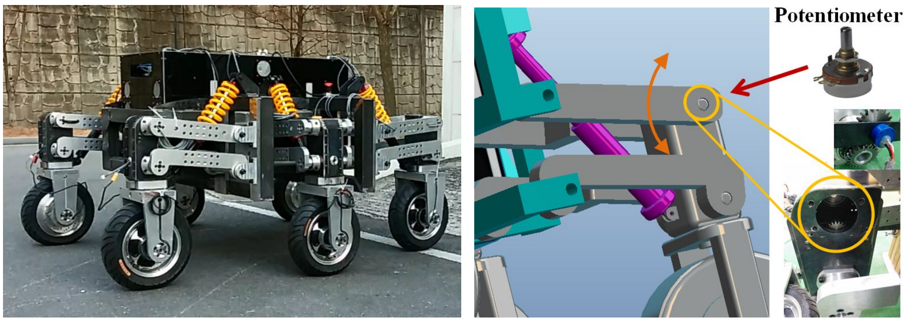


**Fig. 1.** Design of Caleb9 and mounted potentiometer at the end of each arm

**Table 1.** Specification of Caleb9

| **Max Velocity** | 10m/s(40km/h) | **Total Weight** | 800 kg |
|---|---|---|---|
| **Max Slope** | 20˚ | **Operating Time** | 1h 30min |
| **Steering Angle** | - 90˚ ~ 90˚ | **Battery** | Li-ion 48V, 24V |
| **Arm Displacement** | 25cm | **Main Board O/S** | Linux |
| **Robot Size (mm)** | 1460x2180x990 | **Communication** | CAN |

active suspension to adjust damping force (Position Control) and brake module to maintain safety driving (Force Control). Caleb9 can make omnidirectional movement on rough terrains by six driving motors, six steering motors and six semi-active suspensions. Detailed specification is depicted in Table 1.

In a sensor system of caleb9, rotational velocity, torque and steered position of wheel are acquired from feedback data of motor controllers. 3-dimensional position, velocity, acceleration and angle of the robot can be estimated by commercial INS/GPS system on the top of the robot. Arm angles can be measured by potentiometers mounted at the end of each arm as shown in Fig. 1. The potentiometer has a critical role to estimate suspension force and wheel lift by observing changed angle of arms.

### 2.2 Easy Method for Estimation of Suspension Force and Wheel Lift

Suspension force and wheel lift can be estimated from kinematic relation between arm and suspension in Fig. 2. Simply, when the wheel is raised by a force from ground ($L_D$), angle of the arm is changed ($\theta$) and at the same time, the suspension is compressed ($x$) depending on the angle of the arm $\theta$. Once the displacement $x$ of the suspension is known, then suspension force can be easily estimated using (1). In (1), $F_s$ represents suspension force, $K$ is spring coefficient, $C$ is damper coefficient and $\dot{x}$ denotes derivative term of the displacement $x$ with respect to sampling time $\Delta x$ .

$$F_s = Kx + C\dot{x} \tag{1}$$

The displacement $x$ of the suspension can be expressed as a function of angle of the arm $\theta$. In (1), $L_{SI}$ denotes initial total length of the suspension without compression and $L_{SP}$ represents subsequent total length of the suspension with compression. Accordingly, the displacement of the suspension is calculated by

$$x = L_{SI} - L_{SP} \tag{2}$$

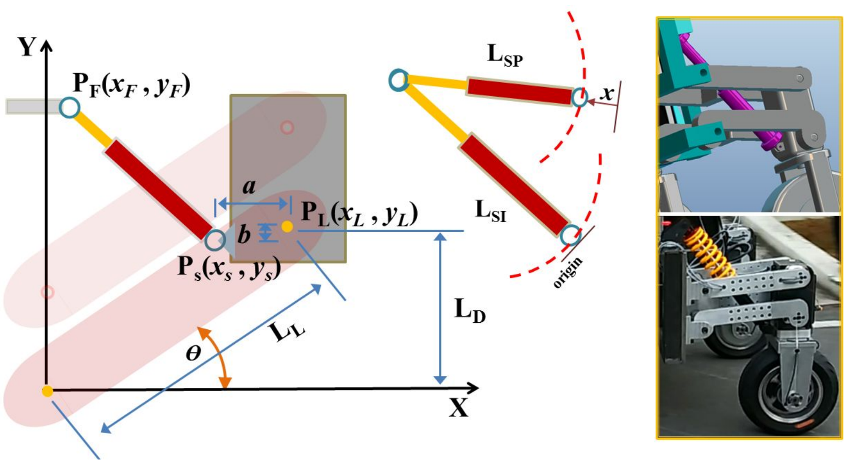


**Fig. 2.** Kinematic relation between arm and suspension

Initial total length of the suspension $L_{SI}$ is given as a constant. Subsequent total length of the suspension $L_{SP}$ is changed depending on the starting position $P_S(x_s, y_s)$ of the suspension which is a function of angle $\theta$ of the arm. In Fig. 2, $P_F(x_F, y_F)$ is the end position of the suspension, $P_L(x_L, x_L)$ represents the end position of arm, $L_L$ denotes length of arm and $a$ is the distance in the $x$-direction between $P_L$ and $P_S$. $b$ represents the distance in the $y$-direction between $P_L$ and $P_S$. $P_F$, $L_L$, $a$ and $b$ are given as a constant from design parameters of caleb9, respectively. $x$-$y$ elements of $P_L$ can be substituted into $x$-$y$ elements of $P_S$ by a and $b$ as follows

$$\mathrm{P_S}(x_s, y_s) = \mathrm{P_L}(x_L - a, x_L - b) \tag{3}$$

And $x$-$y$ elements of $P_L$ are variables to be calculated according to angle $\theta$ of the arm as below

$$\mathrm{P_L}(x_L, y_L); \quad x_L = \mathrm{L_L}\cos(\theta), \quad y_L = \mathrm{L_L}\sin(\theta) \tag{4}$$

For the displacement $x$ of the suspension in (2), $L_{SP}$ can be found by calculating the length between $P_F$ and $P_S$ as

$$\mathrm{L_{SP}} = \sqrt{(x_F - x_s)^2 + (y_F - y_s)^2} \tag{5}$$

Therefore, suspension force can be estimated by (1) based on measurement of angle $\theta$ of the arm.

From estimated suspension force, wheel lift can be easily checked. In Fig. 3, left-side figure describes total forces acting on suspension in the case of contact between wheel and ground (wheel contact). And right-side figure shows total forces acting on suspension in the case of taking wheel off from ground (wheel lift). $F_B'$ is the gross force from robot body, $F_G$ expresses the force from ground, $F_G'$ denotes the rotated force of $F_G$ in the direction of suspension, $F_W$ is the force from wheel part and $F_W'$ denotes the rotated force of $F_W$ in the direction of suspension. In the case of wheel contact, the suspension makes compressed motion and the suspension force can be expressed as the sum of $F_G'$ and $F_B'$. Suspension force $F_s$ is positive by keeping the

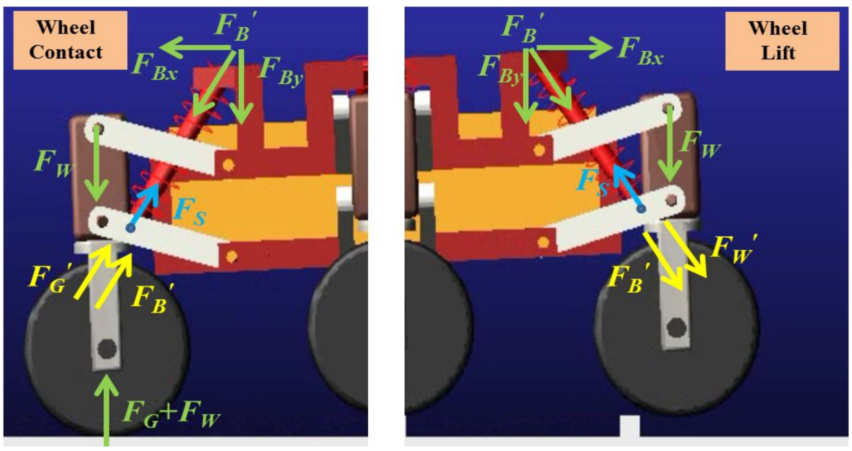


**Fig. 3.** Total forces acting on suspension of caleb9 in case of wheel contact and wheel lift

compressed motion while driving. On the contrary to this, in the case of wheel lift, the suspension makes extension movement and the suspension force can be represented as the sum of $F_W'$ and $F_B'$ in the reverse direction to the suspension force, thereby the suspension force $F_s$ is negative. Additionally, suspension force $F_s$ can be zero in case that the displacement $x$ of the suspension becomes zero by kinematical constraints since the displacement $x$ cannot be changed toward the negative direction. This situation happens when angle of arm is zero by wheel lift. Therefore, it is easy to check the wheel lift by observing negative value and zero value of the suspension force as follows

$$F_s = F_G{}' + F_B{}' \;,\; (F_s > 0) \tag{6}$$

$$F_s = -F_W{}' - F_B{}' \;,\; (F_s \le 0) \tag{7}$$

## 3 Validation of Estimation Method on ADAMS Simulations

The purpose of this simulation is to observe the performance of estimating suspension force and wheel lift in comparison between proposed theory and simulation data on an environment similar to real conditions. ADAMS simulator was used to validate the proposed method on two types of terrains; 1) Hill climbing (30˚) 2) Overcoming obstacles (height 10 and 5 cm, width 5cm) as shown in Fig. 4. The terrain types were selected to observe estimation performance in case of mild changes and rapid changes of suspension force, respectively. In simulations, the velocity of the robot was controlled at 1, 2 and 3m/s in the longitudinal direction and the friction coefficient on the surface was set as 1 to prevent wheel from slippage. And the design parameters of virtual robot in the simulation such as size or weight were determined as the same to the real robot. The spring coefficient and damper coefficient were designated as $K$=8000N/m and $C$ =2200Ns/m. The needed variables to be acquired on simulations are actual angle $\theta$ of arm and ideal suspension force while driving on such terrains and the variables were extracted from simulation data.

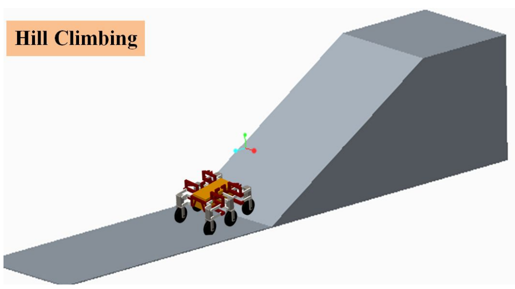


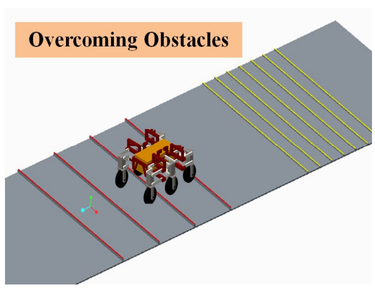


**Fig. 4.** Simulation environments on ADAMS; 1) Hill climbing 2) Overcoming obstacles

### 3.1 Simulation Results in case of Hill Climbing

Figure 5 describes actual angles of right-side arms while climbing a hill at 1m/s. the arm angles are the same to them of left-side arms because the robot moves in the longitudinal direction and the right-side surface shape is also the same to the left-side surface shape. At 0 second, the suspension of the robot takes initial posture without compression. After that time, the robot accelerates the speed to meet desired velocity from around 0 to 5 seconds. Therefore the rear wheel gains more normal force than other wheels and the front wheel gets lowest normal force among them. From the end of the acceleration area, the robot moves with uniform velocity until 15 seconds. From about 15 to 29 seconds, the robot encounters a hill with 30˚ and the angle of arms are significantly changed during hill climbing. The angle of right-middle arm is slightly different with it when the robot does not climb the hill, except for the start and end of the hill. In the vicinity of the start point of the hill, the angle of right-middle arm was reached at zero point as the initial state of the suspension. It can be explained as the wheel was taken off from ground because zero angle of the arm means that normal force was exerted to the wheel. The angle of right-front arm was also reached to zero point during hill climbing. Accordingly, the right-front wheel was lifted off from the surface.

From the angle data in Fig. 5, the suspension force can be estimated by using (1)-(5). Figure 6 shows the estimated data of suspension force in comparison to ideal data of suspension force. Totally, thick lines express the ideal suspension force of right-side arms and thin dot lines represent the estimated suspension force of them. In Fig. 6, it shows that the estimated suspension forces are well-matched with the ideal suspension forces. In case of right-front wheel, the ideal suspension force indicates negative values during hill climbing. However, in the actual situation, the angle of the arm is not changed in the negative direction of the angle as depicted in Fig. 5. The suspension force of right-front and middle wheels are momentarily displayed as negative values because of the term related to the damper in (1), especially $\dot{x}$. But the forces returned soon to the zero line as shown in A of Fig. 6. Wheel lift happened at the right-front and the right-middle wheel as shown that there are the suspensions

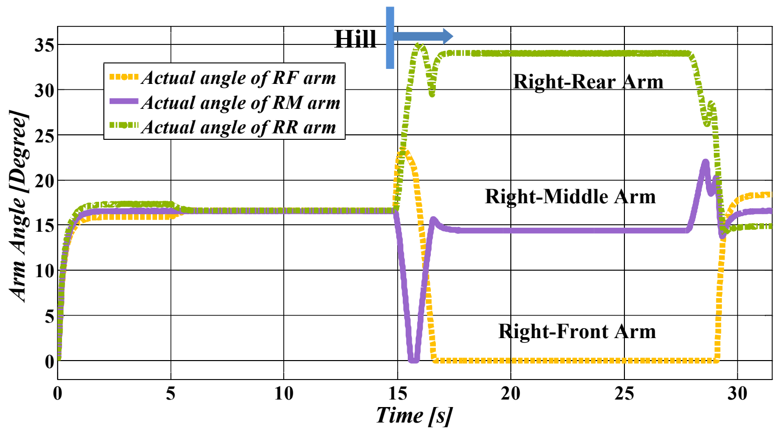


**Fig. 5.** Measured angle of right-side arms while climbing the hill at 1m/s

having negative and zero force values during hill climbing. In comparison to actual motion of the right-front wheel, A region expresses the wheel motion in the vicinity of start point of the hill as described in (a) of Fig. 7 and B region indicates the wheel motion in the vicinity of end point of the hill as depicted in (b) of Fig. 7. In A, at around 15 seconds, the right-middle wheel is lifted off from the surface since the front wheel is faced with the hill and the rear wheel supports the robot against pitch motion of the body. After 1 second, the right-front wheel is taken off from the ground until around the end of the hill as shown that the angle of the arm has zero value after about 16.58 second in (a) of Fig. 7. The right-front wheel contacts to the ground at 29.02 seconds in Fig. 6. The result shows the same performance in (b) of Fig. 7.

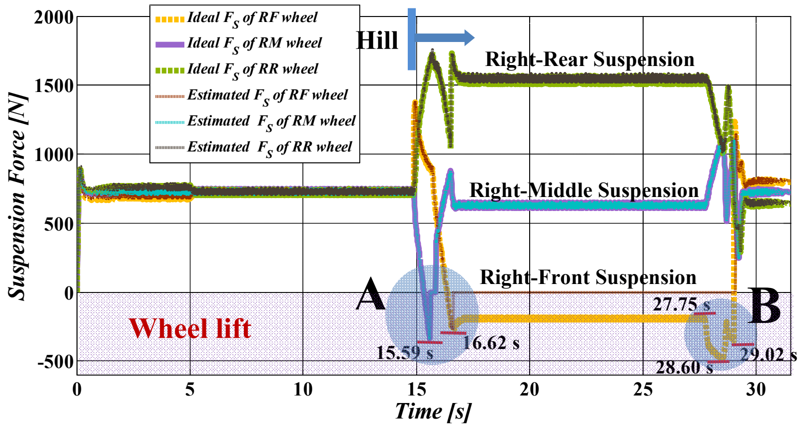


**Fig. 6.** Estimated suspension forces of right-side wheels while climbing the hill at 1m/s

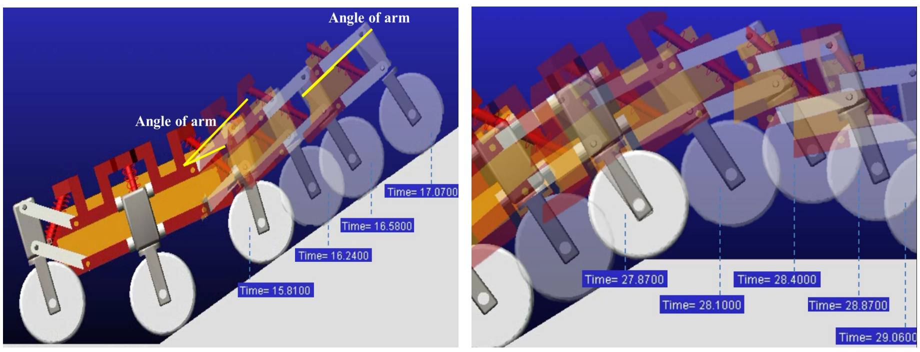


(a) In the vicinity of start point of a hill (b) In the vicinity of end point of a hill

**Fig. 7.** Motion analysis of wheel lift of the right-front wheel while climbing the hill at 1m/s

### 3.2 Simulation Results in case of Overcoming Obstacles

Another simulation was performed to validate the proposed method in a flat surface with obstacles at the robot speed 3m/s. Figure 8 shows the angle of right-side arms while getting over the obstacles. The robot encounters the obstacle with different height (10cm and 5cm). In Fig. 8, during initial 7 seconds, the arm motion is similar to previous motion of arms in Fig. 5 because of the acceleration movement. The RR arm gets the highest angle value among them and the RF arm has the lowest angle value. After 7 seconds, the robot crashes to high obstacles four times and then After 11 seconds, the robot collides with low obstacles seven times. From the front wheel, the arm angle increases in order of position. And the change of the RM arm is the smallest among them. In contrast with the angles of RF and RM arms in Fig. 5, all arm angles of the robot were not converged to zero line in this simulation. From the angle data in Fig. 8, the suspension force of all arms can be also calculated by using (1) - (5) as shown in Fig. 9. Although the angle of arms was not reached to zero line, the estimated suspension forces of all arms are sometimes changed as negative values in both case of being faced with high and low obstacles. As a result, it can be expressed as wheel lift occurs almost eleven times on all obstacles in order to overcome the obstacles.

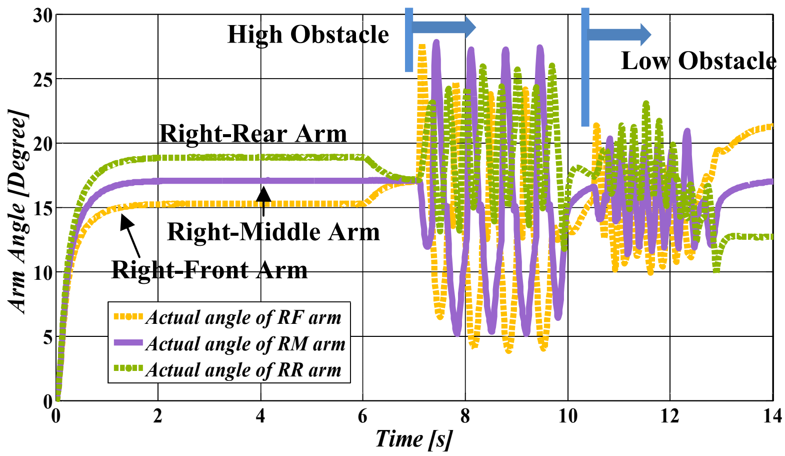


**Fig. 8.** Measured angle of right-side arms while overcoming obstacle at 3m/s

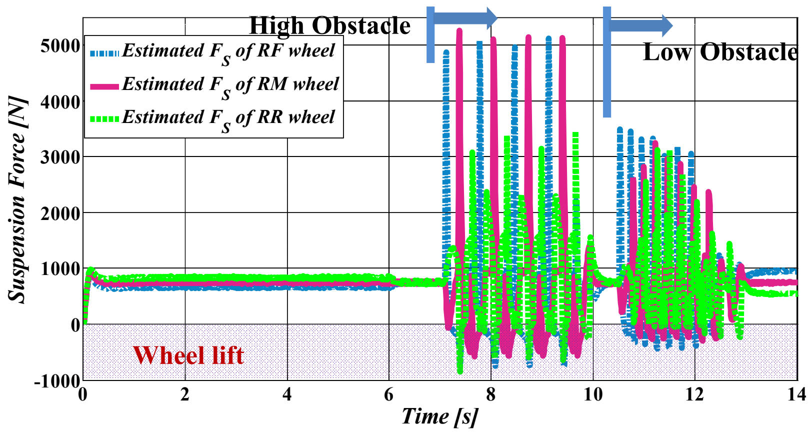


**Fig. 9.** Estimated suspension forces of right-side wheels while overcoming obstacles at 3m/s

For evaluation of validation of measured suspension forces, the wheel motions were analyzed while the robot leaps and bounds over the obstacle. Figure 10 describes the result of comparison between measured suspension force and ideal suspension force of RF wheel. The measured suspension force is well-fitted with ideal one across the board. Figure 11 depicts the RF wheel motion at the analogous moment to C in Fig. 10. The wheel collides with a high obstacle at 9.13 seconds and the wheel is taken off from the obstacle at 9.21 seconds. The wheel reaches the flat surface at 9.48 seconds. The duration of wheel lift is from 9.21 to 9.48 seconds and in Fig. 11, the wheel was lifted off for the similar period to the duration. As the results of the simulations on the hill and the flat surface with obstacles, the proposed method is validated to estimate suspension force and wheel lift of high-speed robot on rough terrain. In the simulations, it was assumed that the angle of all arms, as the key variable for this method, can be accurately measured by a potentiometer mounted at the end of arms and it resulted in such performances as mentioned in the sections for the simulation. For an actual verification on outdoor environments, Caleb9 was applied for getting the data of suspension force and wheel lift in real time on the similar types of surface with simulated environments.

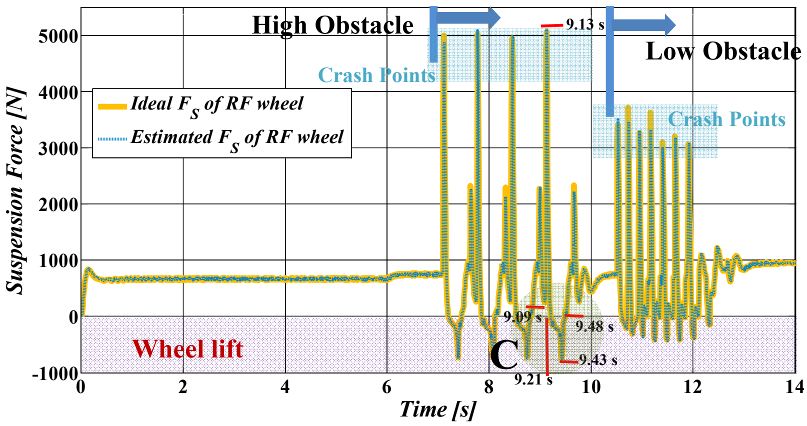


**Fig. 10.** Estimated suspension force of right-front wheel while overcoming obstacles at 3m/s

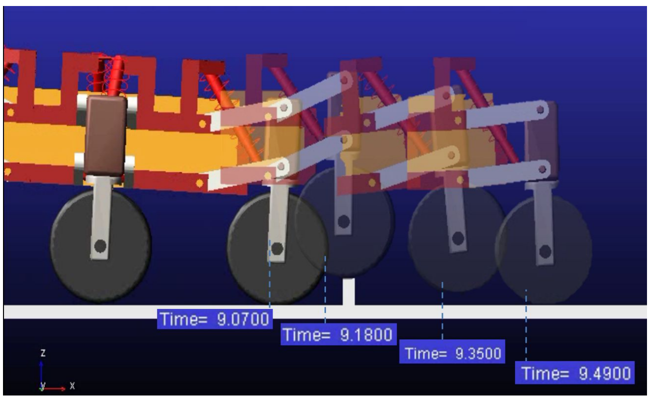


**Fig. 11.** Motion analysis of wheel lift of the RF wheel while overcoming obstacles at 3m/s

# 4 Actual Application of Caleb9 in Outdoor Environments

## 4.1 Experimental Study for Nonlinear Spring and Damper Coefficients

For an actual application of the proposed method, firstly, spring and damper characteristics should be analyzed to set the coefficients of spring and damper because the suspension system is nonlinear unlike conditions in the simulation. For the analysis, a force sensor was installed at the end of the suspension on the RR wheel to acquire exact data of suspension force in the same direction to the suspension motion as shown in Fig. 12. The suspensions mounted on Caleb9 are customized products by a company named 'J5 Suspension'. Accordingly, the data related to spring and damper characteristics can be obtained from the company. Figure 13 and 14 describe the data of spring and damping force depending on the displacement x and the damping velocity $\dot{x}$, respectively. From the data of Fig. 13 and Fig 14, the spring-damper equations can be derived by a nonlinear regression technique using polynomial equations of (9) – (11). Equation (9) represents the spring force as a function of the displacement $x$ and equations (10) – (11) indicate the damping force as functions of the damping velocity $\dot{x}$. In (10) – (11), the damping force is divided into two cases of compression ($C_{ext}$) and extension ($C_{com}$) of the suspension and it can be determined by observing the positive and negative sign of the damping velocity $\dot{x}$. In (9) –(11), the polynomial constants are $K_1$=5.9694e+5, $K_2$=-3.5295e+6, $K_3$=1.1493e+6, $K_4$=0.0531e+6, $K_5$=0.0011e+6, $C_{com1}$=6000, $C_{com2}$=2.89e+3, $C_{com3}$=-1.0875e+3, $C_{com4}$=0.7289e+3, $C_{com5}$=0.0509e+3, $C_{ext1}$=17000, $C_{ext2}$=0.6463e+3, $C_{ext3}$=-2.5403e+3, $C_{ext4}$=4.4513e+3, $C_{ext5}$=0.1142e+3, respectively. Therefore, the suspension force can be estimated by (8).

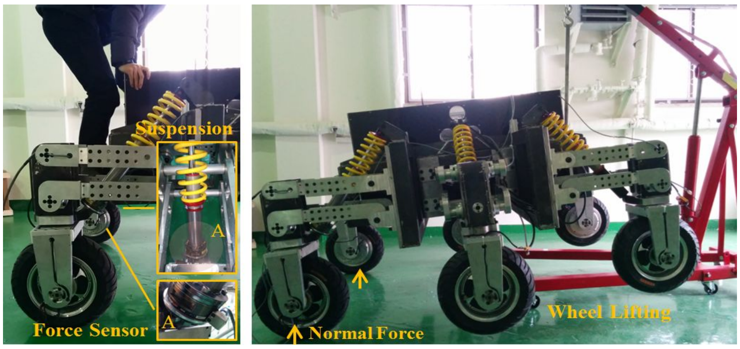


**Fig. 12.** Suspension test to determine spring and damper coefficients on the RR wheel

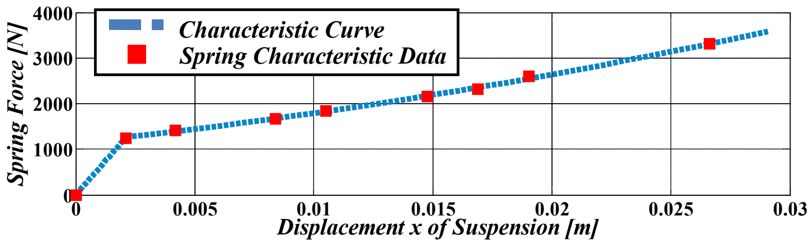


**Fig. 13.** The spring force depending on the displacement $x$ of the suspension

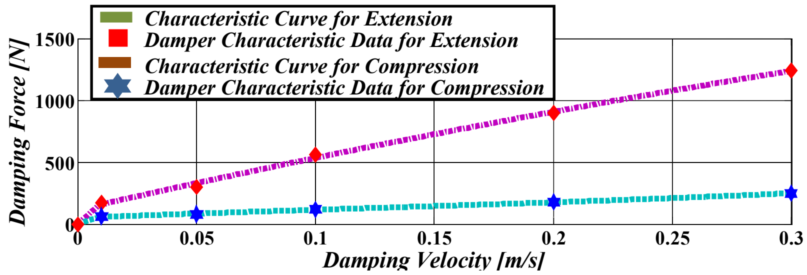


**Fig. 14.** The damping force depending on damping velocity $\dot{x}$ of the suspension

$$F_s = F_{spring} + F_{damper} \tag{8}$$

$$\begin{aligned} F_{spring} &= K_1 x\,, && if\ x < 0.0021\,[m] \\ F_{spring} &= K_2 x^3 + K_3 x^2 + K_4 x + K_5\,, && if\ x \geq 0.0021\,[m] \end{aligned} \tag{9}$$

$$if\ \dot{x} \geq 0 \begin{cases} F_{damping} = C_{com1}\dot{x}\,, & if\ \dot{x} < 0.01\,[m/s] \\ F_{damping} = C_{com2}\dot{x}^3 + C_{com3}\dot{x}^2 + C_{com4}\dot{x} + C_{com5}\,, & if\ \dot{x} \geq 0.01\,[m/s] \end{cases} \tag{10}$$

$$if\ \dot{x} < 0 \begin{cases} F_{damping} = C_{ext1}\dot{x}\,, & if\ |\dot{x}| < 0.01\,[m/s] \\ F_{damping} = C_{ext2}\dot{x}^3 + C_{ext3}\dot{x}^2 + C_{ext4}\dot{x} + C_{ext5}\,, & if\ |\dot{x}| \geq 0.01\,[m/s] \end{cases} \tag{11}$$

For verifying the validity of the equations related to the suspension force, two types of tests were performed; a changing force test (the right-side figure in Fig. 12) and a jump test (the left-side figure in Fig. 12). The changing force test is for only reviewing spring characteristics without a damper effect by slowly changing the displacement $x$ of the suspension. Figure 15 shows the arm angle of the right-side wheels. The angle of the RM and RF arms are zero since the RM and RF wheel were lifted off from the surface. But the angle of the RR arm is gradually changed four times (case 1~4) by concentrated weight of the robot on the rear-side wheels while tilting the body by a crane. Figure 16 depicts the estimated suspension force of the right-side wheels in comparison to the ideal suspension force by the force sensor on the RR wheel. In Fig. 16, the estimated $F_S$ is well matched with the ideal $F_S$ in spite of changing cases from 1 to 4 and it shows that the RM and RF wheels were taken off from the ground. The jump test is for comprehensively reviewing spring-damper characteristics by periodically jumping on the rear of the robot body. Figure 17 shows that the actual $F_S$ is closely estimated to the ideal $F_S$ throughout the test despite of rapidly changing the force by jump.

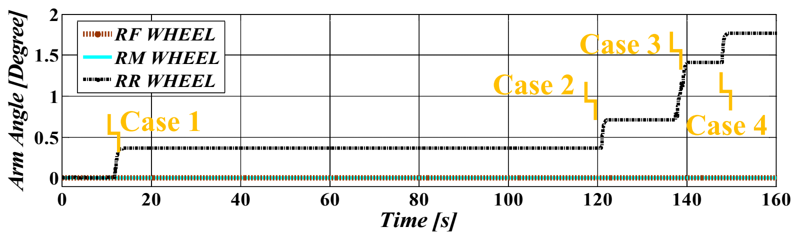


**Fig. 15.** The arm angle of the right-side wheels under normal force on the RR wheel

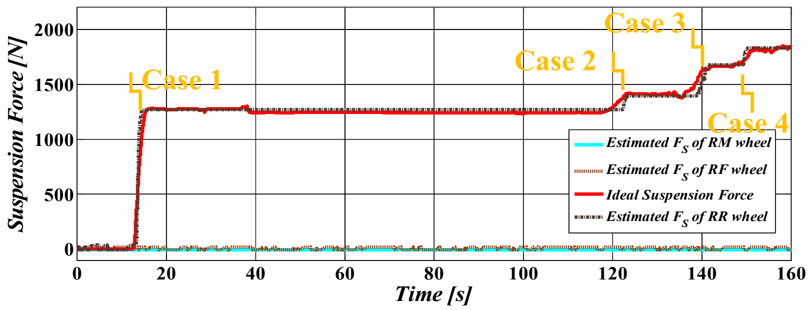


**Fig. 16.** Comparison between estimated and ideal suspension force using the data in Fig. 13

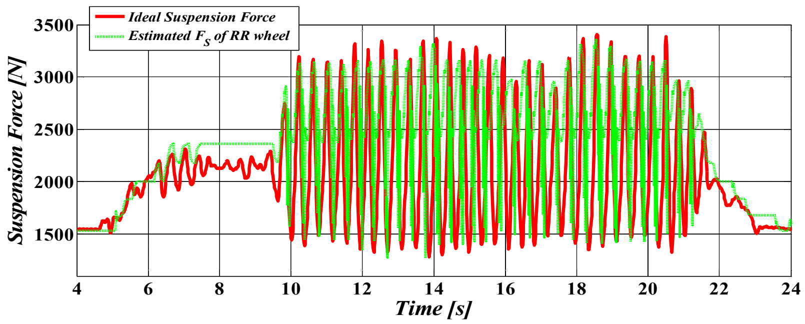


**Fig. 17.** Verification of estimated suspension force through jump test

### 4.2 Experimental Results of Estimation of Suspension Force and Wheel Lift

In order to verify the performance in an actual environment, an outdoor experiment was conducted using Caleb9 on a surface with an obstacle (inclined surface with 25 degrees) as shown in the left-bottom figure of Fig. 18. The robot was moved backward at almost 3m/s and the wheels move as from A step to B step while

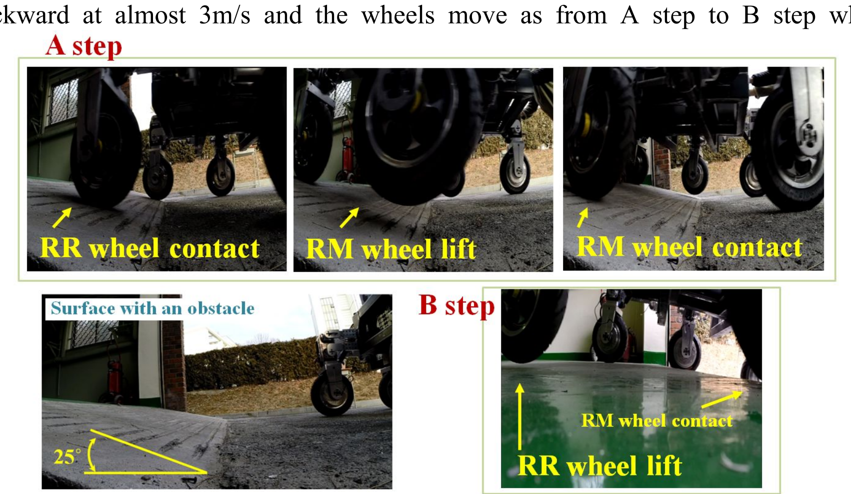


**Fig. 18.** An experimental environment to verify the performance of the proposed method

overcoming the obstacle. In A step, firstly, the RR wheel encountered the obstacle and secondly, the RM wheel was lifted off by the effect of the surface shape although the RR and RF wheel contacted to the surface. Finally, the RM wheel was reached on the ground. And then, In B step, the RR wheel was also taken off by the force on the RM wheel supported the robot weight at the surface of the obstacle. The process of the motion from A step to B step is described as the measured data of the angle of the right-side arms as depicted in Fig. 19. In A step of Fig. 19, the angle of the RR and RF arms increased by the collision with the obstacle, thereby the angle of the RM arm was converged to the zero point which means wheel lift. And in B step of Fig. 19, the RM wheel was colliding with the obstacle and the angle of RM arm increased sharply for the moment, thereby the angle of the RR and RF arms was reached to the zero line for about 0.3 seconds. The validity of the results can be verified in Fig. 20. In Fig. 20, the estimated $F_S$ of the RR wheel increases until 3000 N (collision) and decreases until 0 N (wheel lift). After overcoming the obstacle, the estimated $F_S$ returns to the initial suspension force. In comparison between the estimated and the ideal $F_S$ in Fig. 20, it shows that the estimated physical phenomenon is quite analogous to the ideal one. And also, these motions of the wheel and the arms are considerably similar to the simulations of the hill climbing in Fig. 5 – 7.

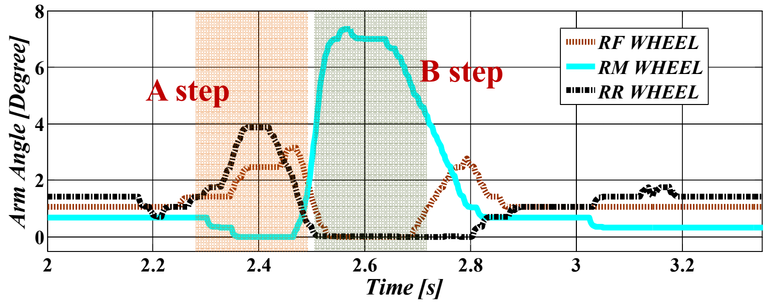


**Fig. 19.** Measured angle of the right-side arms while overcoming an obstacle at 3m/s

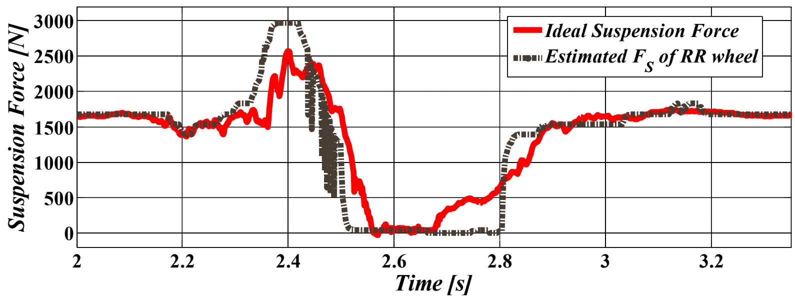


**Fig. 20.** Estimated suspension force of the right-rear wheel under the experimental conditions

## 5 Conclusion

For actual applications of rough terrain robots, it is important to know the present state of wheels, especially wheel lift and suspension force related to wheel traction and body stability, to maintain optimized maneuverability. For this reason, this paper proposed the easy way to estimate wheel lift and suspension force of a high-speed wheeled robot (Caleb9) on uneven surfaces. For the achievement of this goal, the inexpensive potentiometer was applied to estimate the wheel lift and suspension force by measuring the angle of each arm in real-time. And also, the simple spring-damper system was employed and the equations related the suspension was derived based on the data which was provided by the company named ‘J5 Suspension’. The proposed method was validated through two types of simulations on the environments; hill climbing and overcoming obstacles and also, it was verified through actual experiments of overcoming the inclined surface.

As future works, in the outdoor mobile robotics, it is of great importance to predict stabilities for traction of wheel and rollover of body. Such the studies are closely related to the researches of measuring the normal force or the suspension force. Therefore, the proposed method in this paper can be employed in dynamical outdoor environments in order to evaluate the stability based on the more exact force data from this method than estimating actual force using dynamic models.

**Acknowledgments.** The authors gratefully acknowledge the support from UTRC(Unmanned Technology Research Center) at KAIST(Korea Advanced Institute of Science and Technology) originally funded by DAPA, ADD.

## References

1. Jayoung Kim and Jihong Lee, “Intelligent Slip-Optimization Control with Traction-Energy Trade-off for Wheeled Robots on Rough Terrain”, IEEE/RSJ International Conference on Intelligent Robots and Systems(IROS), 2014.
2. Ambroise Krebs, Fabian Risch, Thomas Thueer, Jerome Maye, Cedric Pradalier and Roland Siegwart, “Rover control based on an optimal torque distribution – Application to 6 motorized wheels passive rover”, IEEE/RSJ International Conference on Intelligent Robots and Systems(IROS), 2010.
3. Nicolas Bouton, Roland Lenain, Benoit Thuilot and Philippe Martinet, “A new device dedicated to autonomous mobile robot dynamic stability: Application to an off-road mobile robot”, IEEE International Conference on Robotics and Automation(ICRA), 2010.
4. Steven C. Peters and Karl Iagnemma, “Stability measurement of high-speed vehicles”, Journal of Vehicle System Dynamics, Vol. 47, No. 6, pp.701-720, 2009.
5. Moshe Mann and Zvi Shiller, “Dynamic Stability of Off-Road Vehicles: Quasi-3D Analysis”, IEEE International Conference on Robotics and Automation(ICRA), 2008.
6. Moustapha Doumiati, Ali Charara Alessandro Victorino and Daniel Lechner, “Vehicle Dynamics Estimation using Kalman Filtering”, Automation – Control and Industrial Engineering Series, 2013.
7. Genya Ishigami, Gaurav Kewlani, and Karl Iagnemma, “Statistical Mobility Prediction for Planetary Surface Exploration Rovers in Uncertain Terrain”, IEEE International Conference on Robotics and Automation(ICRA), 2010.
8. Sang Hyun Joo, Jeong Han Lee, Yong Woon Park, Wand Suk Yoo and Jihong Lee, “Real time traversability analysis to enhance rough terrain navigation for an 6x6 autonomous vehicle”, Journal of Mechanical Science and Technology, Vol. 4, No. 27, pp. 1125-1134, 2013.
9. Matthew Spenko, Yoji Kuroda, Steven Dubowsky, and Karl Iagnemma, “Hazard Avoidance for High-Speed Mobile Robots in Rough Terrain”, Journal of Field Robotics, Vol. 5, No. 23, pp. 311-331, 2006.
10. Mohamed Krid and Faiz Benamar, “Design and control of an active anti-roll system for a fast rover”, IEEE/RSJ International Conference on Intelligent Robots and Systems(IROS), 2011.